Supplement of

High atmospheric oxidation capacity drives wintertime nitrate pollution in the eastern Yangtze River Delta of China

Han Zang[1], Yue Zhao[1,*], Juntao Huo[2], Qianbiao Zhao[2], Qingyan Fu[2], Yusen Duan[2,*], Jingyuan Shao[3], Cheng Huang[4], Jingyu An[4], Likun Xue[5], Ziyue Li[1], Chenxi Li[1], Huayun Xiao[1]

[1]School of Environmental Science and Engineering, Shanghai Jiao Tong University, Shanghai, 200240, China
[2]Shanghai Environmental Monitoring Center, Shanghai 200235, China
[3]College of Flight Technology, Civil Aviation University of China, Tianjin 300300, China
[4]Shanghai Academy of Environmental Sciences, Shanghai 200233, China
[5]Environment Research Institute, Shandong University, Qingdao, Shandong, 266237, China

*Correspondence: Yue Zhao (yuezhao20@sjtu.edu.cn); Yusen Duan (duanys@yeah.net)

S1. Hygroscopicity correction of aerosol volume and surface area concentrations

The hygroscopicity parameter kappa (κ) of ambient particles was evaluated based on the measured chemical composition and an empirical parameterization proposed by Liu et al. (2014):

$$\kappa = 0.01 + 0.63f\mathrm{NH_4^+} + 0.51f\mathrm{NO_3^-} + 0.81f\mathrm{SO_4^{2-}} + 0.18f\mathrm{WSOC} \quad \text{(S1)}$$

where *f*x represents the mass fraction of component x in the particles. During the observation period, the mass fraction of OC in $PM_{2.5}$ was 8-13% when $PM_{2.5}$ mass concentration was above 35 μg m^{-3}, and the water soluble fraction (WSOC) could be smaller. Therefore, we did not consider the contribution of WSOC to κ in our study.

According to the definition of κ (Farmer et al., 2015), we can get the diameter of the wet particle:

$$\frac{\mathrm{RH}}{100} = \frac{D_{p,wet}^3 - D_{p,dry}^3}{D_{p,wet}^3 - (1-\kappa)D_{p,dry}^3}\exp\left(\frac{4\sigma_s M_w}{\mathrm{RT}\rho_w D_{p,dry}}\right) \quad \text{(S2)}$$

Where $D_{p,dry}$ and $D_{p,wet}$ are the dry and wet diameters of particle, respectively; σ_s is surface tension of the solution/air interface; ρ_w and M_w are the density and molecular weight of water; R is the ideal gas constant and T is the temperature (in K).

S2. The parameterization of the major heterogeneous production pathways of HONO

In this study, we parameterized the major heterogeneous HONO production pathways to estimate the HONO budget during the pollution episodes (see Table 1 in the main text). For the photolysis frequency of particulate nitrate (jNO_3^-), previous studies suggested that it had a similar diurnal variation with the photolysis frequency of HNO_3 (Romer et al., 2018; Xue et al., 2020). Considering the fact that the photolysis rate of particulate nitrate is faster than that of HNO_3, an enhancement factor (EF= $jNO_3^-/jHNO_3$) was employed to parameterized the photolysis process of particulate nitrate. We also added the heterogeneous reaction between SO_2 and NO_2 on aqueous aerosols (R.S1), which is also a source of HONO in the atmosphere (Wang et al., 2016; Wang et al., 2020). In the model, the rate of this reaction was calculated using eq. S3:

$$SO_2\,(g) + 2NO_2\,(g) + 2H_2O\,(aq) \rightarrow SO_4^{2-}\,(aq) + 2\,H^+\,(aq) + 2\,HONO\,(g) \quad \text{(R.S1)}$$

$$k_{10} = k_{aq} \times H_{SO_2} \times H_{NO_2} \times \left(1 + \frac{K_{\alpha1}}{[\mathrm{H^+}]} + \frac{K_{\alpha1} \times K_{\alpha2}}{[\mathrm{H^+}]^2}\right) \times \mathrm{ALWC} \times 10^{-9} \quad \text{(S3)}$$

where k_{aq} is the aqueous reaction rate of SO_2 and NO_2, which is 1.4 × 10^5 M^{-1} s^{-1} for pH < 5 and 2 × 10^6 M^{-1} s^{-1} for pH > 6, with a linear interpolation between the two pH values (Lee and Schwartz, 1983; Wang et al., 2020); H_{SO2} and H_{NO2} are the Henry's Law coefficient of NO_2 and SO_2 in water, with a value of 1.23 M atm^{-1} and 1.2×10^{-2} M atm^{-1} at 298K, respectively; $K_{\alpha1}$ and $K_{\alpha2}$ are the first- and second-order dissociation constant of $SO_2 \cdot H_2O$, with a value of 1.3×10^{-2} and 6.6×10^{-8} at 298K, respectively. The *H* values at various temperatures can be derived by eq. S4:

$$H_T = H_{298}\exp\left(\frac{\Delta \mathrm{H_A}}{\mathrm{R}}\left(\frac{1}{298} - \frac{1}{T}\right)\right) \quad \text{(S4)}$$

Where ΔH_A is the enthalpy change of dissollution at constant temperature and pressure. At 298 K, the value of ΔH_A is -6.25 kcal mol^{-1} for SO_2 and -5.0 kcal mol^{-1} for NO_2 (Seinfeld and Pandis, 2016). T is the temperature (in K).

In addition, the dissociation constant of $SO_2 \cdot H_2O$ at different temperatures can be derived by eq. S5:

$$K_T = K_{298}\exp(\frac{\Delta H}{R}(\frac{1}{298}-\frac{1}{T})) \quad (S5)$$

Where ΔH is the enthalpy change of dissociation at constant temperature and pressure. At 298 K, the value of ΔH is -4.16 and -2.23 kcal mol^{-1} for disocciation of $SO_2 \cdot H_2O$ and HSO_3^-, respectively (Seinfeld and Pandis, 2016).

We also considered the direct emissions of HONO from vehicles based on a 4 km × 4 km emission inventory of NO_x and an empirical emission ratio (0.8%) of HONO to NO_2 (Kurtenbach et al., 2001; An et al., 2021).

S3. Analysis of the time series of pollutants at the Qingpu site in the winter of 2019

The time series of $PM_{2.5}$, nitrate, and other related parameters at the Qingpu site in 2019 are shown in Figure S2. The variation trends of the pollutants at the Qingpu site were similar to those at the Pudong site, but the concentrations were much higher. Nitrate was also the dominant component in $PM_{2.5}$ during the pollution episodes, and the relatively higher nitrate concentration at the Qingpu site might be due to the higher NO_x emissions (8-263 ppb). The O_3 concentration ranged between 1-65 ppb with an average of 22 ppb. The O_x concentration ranged from 22 to 85 ppb and was often higher than 40 ppb during the observation period. The high atmospheric oxidation capacity led to the high NOR at the Qingpu site, which was up to 0.54. Similarly, the ALWC was also high due to the high RH in the eastern YRD, and sometimes could also exceed 200 μg m^{-3}, which would make an important contribution to the nitrate formation.

S4. Case studies of the model simulation during the pollution episodes at the Qingpu site

Different from the Pudong site, the increase of nitrate concentration at the Qingpu site in case 1 occurred during the daytime, from 19.2 μg m^{-3} at 6:00 to 39.1 μg m^{-3} at 14:00 on 30 December, 2019, with an average growth rate of 2.5 μg m^{-3} h^{-1} (Figure S6a). The OH radical concentrations was high during the nitrate-increasing period, and the maximum values even reached 2.9×10^6 molecules cm^{-3}, while the N_2O_5 concentration was close to 0 ppb. This high OH concentration made the gas-phase OH + NO_2 process a dominant nitrate formation pathway in this case. After excluding data under RH > 95% conditions, the simulated average production rate of HNO_3 from the gas-phase OH + NO_2 process during the daytime reached 6.9 μg m^{-3} h^{-1}.

In episode 2 (see Figure S6b), the nitrate concentration was maintained at a high level (30-40 μg m^{-3}) from the noon of 11 January to the midnight of 14 January, 2020. It then had a rapid increase from 36.1 μg m^{-3} at 01:00 to 74.9 μg m^{-3} at 10:00 on 14 January, 2020, with an average growth rate of 4.3

μg m^{-3} h^{-1}. Similar to the Pudong site, the heterogeneous hydrolysis of N_2O_5 made the major contribution to the HNO_3 formation during this episode, with the average production rate of 4.0 μg m^{-3} h^{-1}, twice that by the gas-phase process.

S5. Sensitivity analyses for key parameters of heterogeneous HONO formation in the model

As significant uncertainties remain in the key parameters of the heterogeneous HONO formation pathways used in the model (see Table 1 in the main text), which could affect the prediction of the OH concentration and thereby HNO_3 production via gas-phase OH + NO_2 reaction, we conducted sensitivity analyses for such parameters to evaluate their influences on HNO_3 production during two typical pollution episodes at the Pudong site (see Figure S8). In the base case simulation where a best guess of kinetic parameters was used (see Table 1), the formation of nitrate had comparable contributions from the gas-phase and heterogeneous processes (45% vs. 53%) during the episode 1, while it was dominated by the heterogeneous process (79%) during episode 2. The sensitivity analyses show that although the dark uptake coefficient of NO_2 on ground surfaces (γNO_2-dk-gs) had the largest influence on HONO concentration during nighttime (-40%/+196%, Figures S8a, d), the photo-enhanced uptake coefficient of NO_2 on ground surfaces (γNO_2-hv-gs) had the greatest influence on the overall HONO formation as well as HNO_3 production via the gas-phase process (Figures S8b, c, e, f). Specifically, varying the γNO_2-hv-gs value by a factor of 5, the gas-phase HNO_3 production rate had a change within -13%/+38% and -22%/+63% compared to the base scenario for the episodes 1 and 2, respectively. Correspondingly, the contribution of gas-phase processes to the total HNO_3 formation varied within -3%/+8% and -4%/+8%, respectively. It should be noted that variations in these kinetic parameters did not significantly affect heterogeneous HNO_3 production. These results suggest that the parameterizations of the heterogeneous HONO formation pathways in the model could provide robust constraints on the relative contributions of both gas-phase and heterogeneous processes to nitrate formation during haze pollution events.

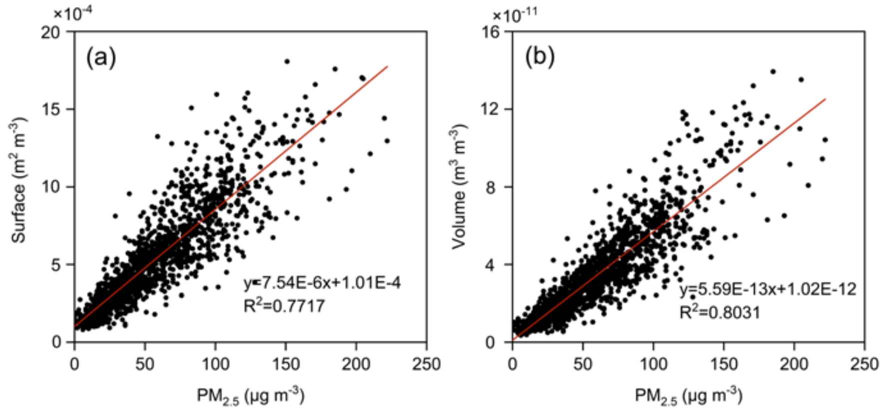

Figure S1 (a) surface area and (b) volume concentrations of dry $PM_{2.5}$ as a function of $PM_{2.5}$ mass concentration at the Qingpu site in 2019.

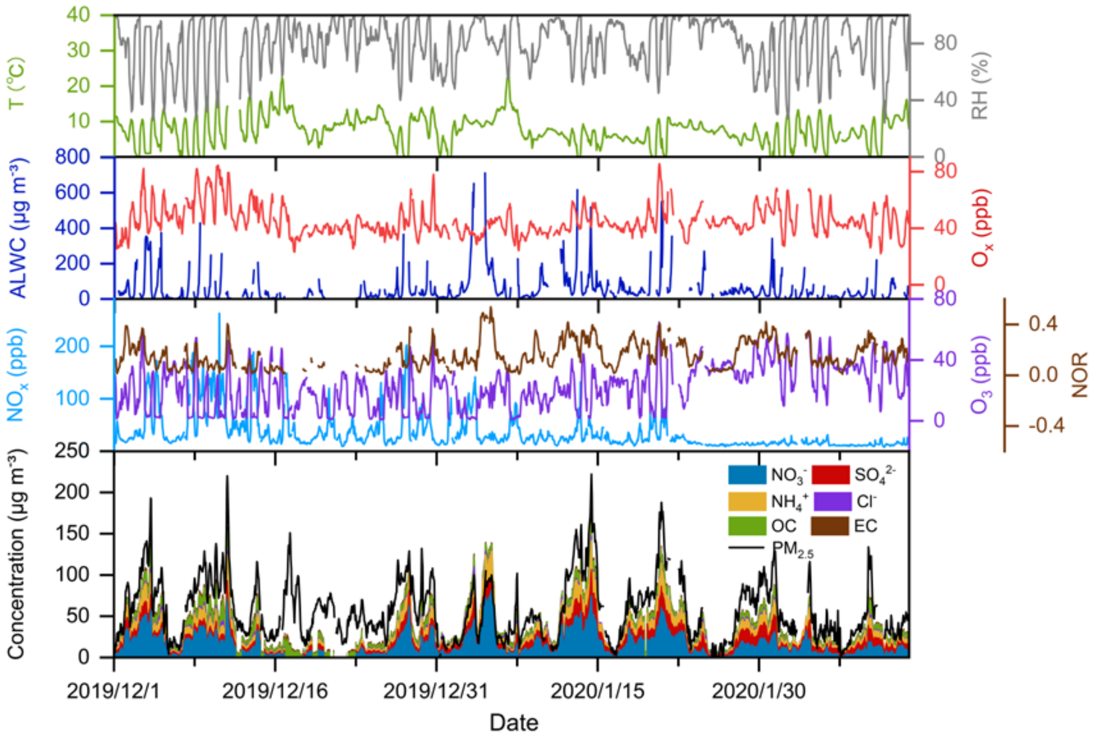

Figure S2 Time series of temperature, relative humidity (RH), aerosol liquid water content (ALWC), NO_x, O_3, O_x, nitrogen oxidation ratio (NOR), as well as $PM_{2.5}$ and major particulate compositions at the Qingpu site in winter 2019.

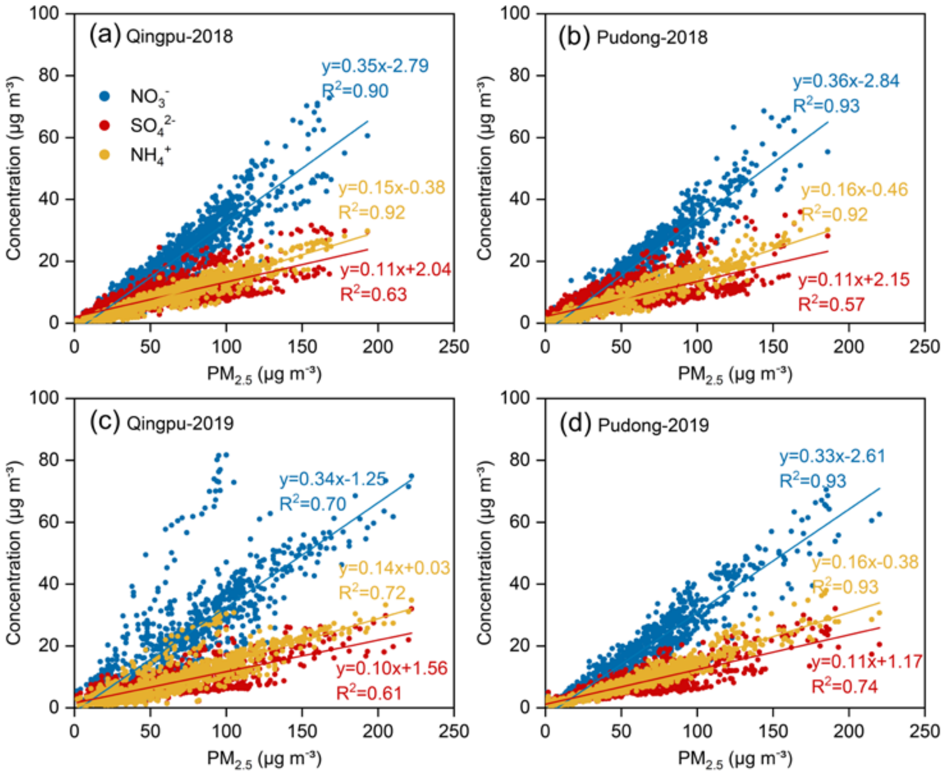

Figure S3 Correlation between the concentrations of $PM_{2.5}$ and nitrate, sulfate and ammonium.

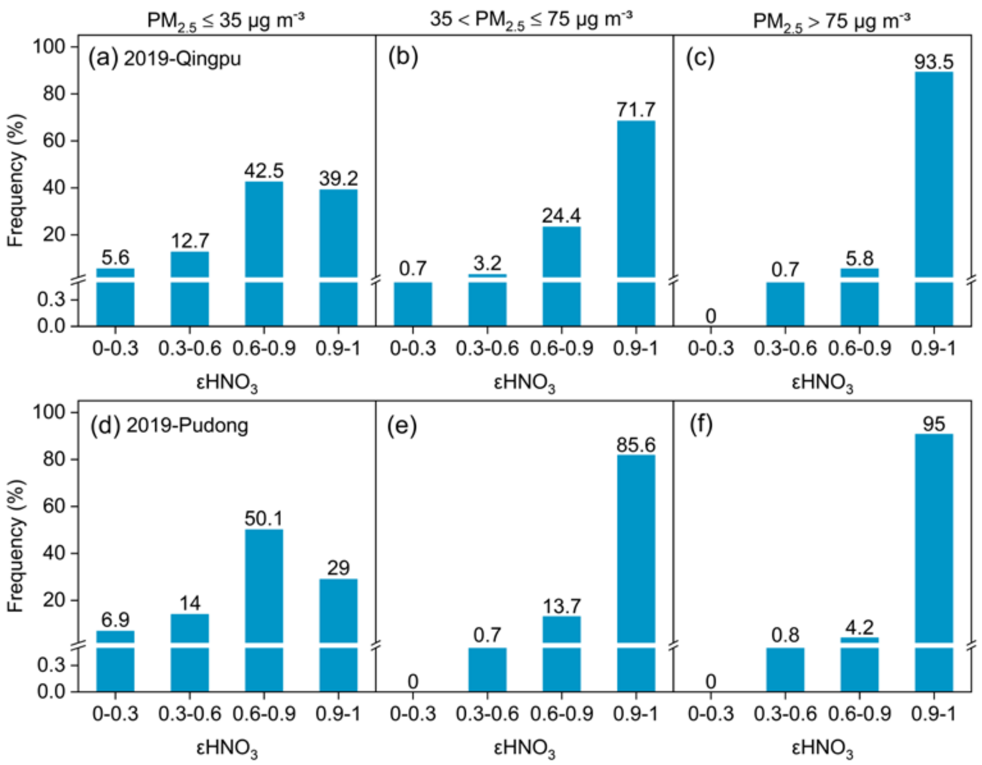

Figure S4 Frequency distribution of εHNO_3 under different $PM_{2.5}$ pollution conditions at (a-c) Qingpu and (d-f) Pudong sites during winter 2019.

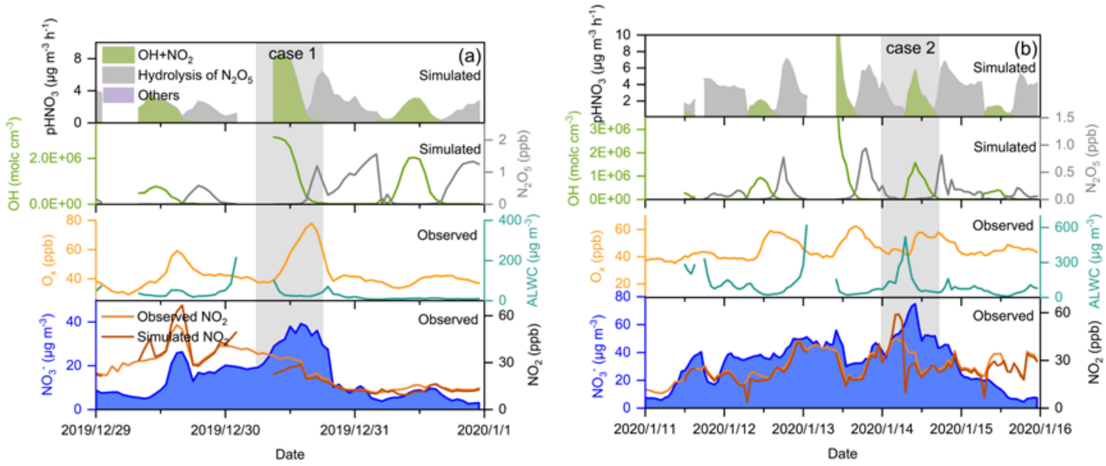

Figure S5 Time series of particulate nitrate, NO_2, O_x, ALWC, OH, N_2O_5, as well as the formation rates of HNO_3 from different processes during the two selected pollution episodes at the Qingpu site in 2019. The simulated data with RH > 95% were not included in the figure.

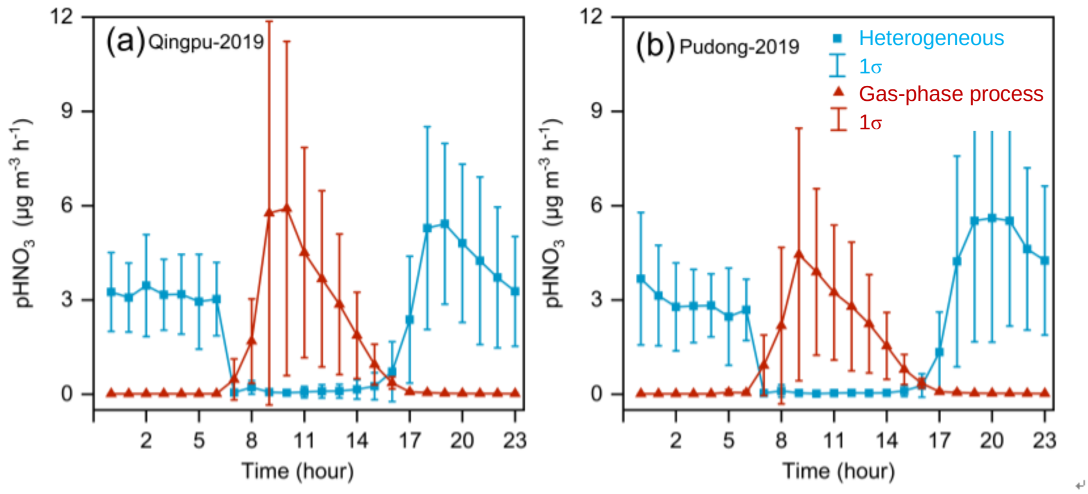

Figure S6 Average diurnal profile of HNO_3 production rates from the heterogeneous and gas-phase processes during all the six pollution episodes at (a) Qingpu and (b) Pudong sites.

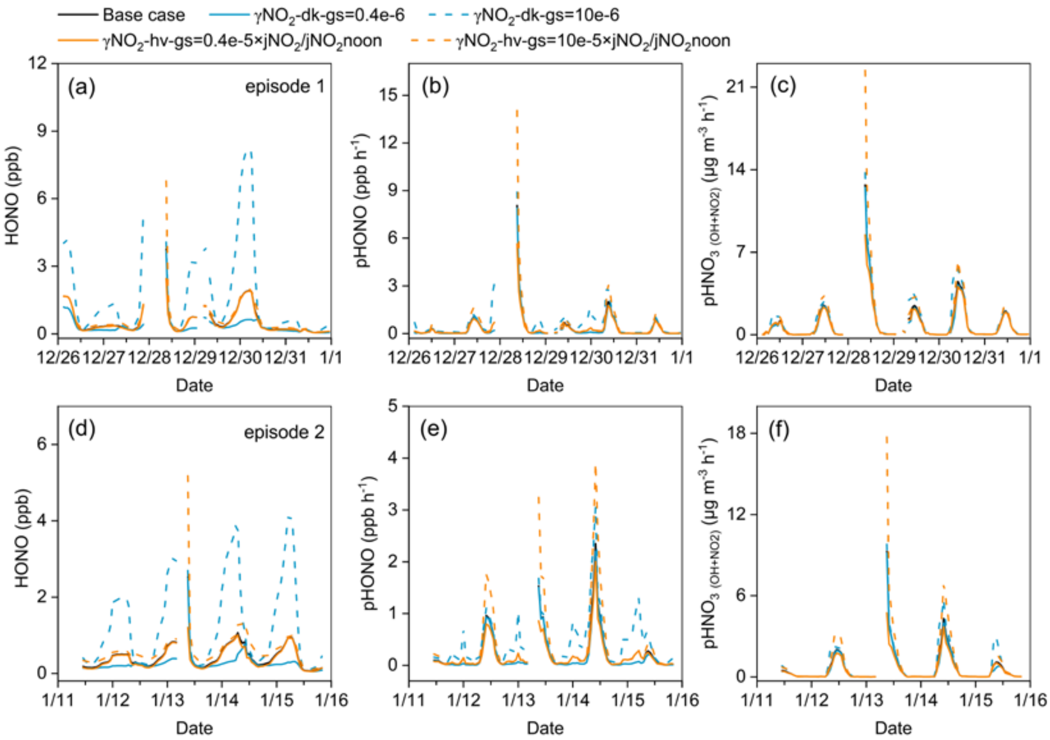

Figure S7 Sensitivity of (a, d) HONO concentration and production rates of (b, e) HONO and (c, f) HNO_3 to the variations in the values of key parameters of the heterogeneous HONO formation pathways in the model. Episode 1 (a-c) was from 26 to 31 December, 2019. Episode 2 (d-f) was from 11 to 15 January, 2020. The base case was simulated using the best guess of the parameters as listed in Table 1 in the main text.

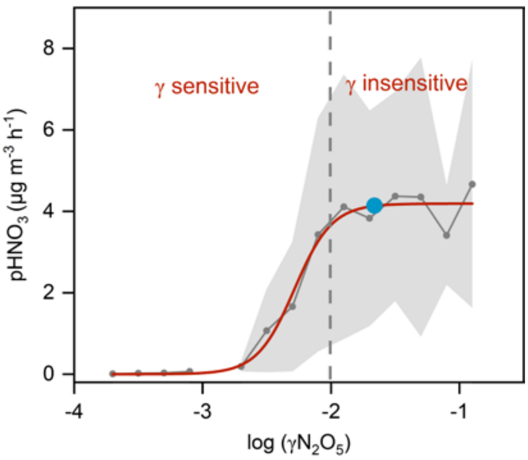

Figure S8 Production rate of HNO_3 from the heterogeneous hydrolysis of N_2O_5 (the grey line with markers) as a function of γN_2O_5 during the six haze pollution episodes at the Pudong site in the winter of 2019 (not including the data with RH > 95%). The red line is an "S" curve fitted to the HNO_3 production rate and the shaded area is the standard deviation. The blue circle indicates the median of γN_2O_5 (0.022) during the six pollution episodes, which is located in the region where the heterogeneous production of HNO_3 is insensitive to the variation in the value of γN_2O_5. This suggests that the uptake of N_2O_5 by aerosols was very efficient so that it was not the rate-determining step in the heterogeneous HNO_3 formation during the haze pollution periods.

References:

An, J., Huang, Y., Huang, C., Wang, X., Yan, R., Wang, Q., Wang, H., Jing, S. a., Zhang, Y., and Liu, Y.: Emission inventory of air pollutants and chemical speciation for specific anthropogenic sources based on local measurements in the Yangtze River Delta region, China, Atmos. Chem. Phys., 21, 2003-2025, doi, 2021.

Farmer, D. K., Cappa, C. D., and Kreidenweis, S. M.: Atmospheric Processes and Their Controlling Influence on Cloud Condensation Nuclei Activity, Chem. Rev., 115, 4199-4217, doi: 10.1021/cr5006292, 2015.

Kurtenbach, R., Becker, K., Gomes, J., Kleffmann, J., Lörzer, J., Spittler, M., Wiesen, P., Ackermann, R., Geyer, A., and Platt, U.: Investigations of emissions and heterogeneous formation of HONO in a road traffic tunnel, Atmos. Environ., 35, 3385-3394, doi, 2001.

Lee, Y., and Schwartz, S. E.: Kinetics of oxidation of aqueous sulfur (IV) by nitrogen dioxide, Precipitation Scavenging, Dry Deposition and Resuspension, 1, 453-470, doi, 1983.

Liu, H. J., Zhao, C. S., Nekat, B., Ma, N., Wiedensohler, A., van Pinxteren, D., Spindler, G., Muller, K., and Herrmann, H.: Aerosol hygroscopicity derived from size-segregated chemical composition and its parameterization in the North China Plain, Atmos. Chem. Phys., 14, 2525-2539, doi: 10.5194/acp-14-2525-2014, 2014.

Romer, P. S., Wooldridge, P. J., Crounse, J. D., Kim, M. J., Wennberg, P. O., Dibb, J. E., Scheuer, E., Blake, D. R., Meinardi, S., and Brosius, A. L.: Constraints on Aerosol Nitrate Photolysis as a Potential Source of HONO and NO x, Environ. Sci. Technol., 52, 13738-13746, doi, 2018.

Seinfeld, J. H., and Pandis, S. N.: Atmospheric chemistry and physics: from air pollution to climate change, Third edition. ed., John Wiley & Sons, Inc., Hoboken, New Jersey, xxvi, 1120 pages pp., 2016.

Wang, G., Zhang, R., Gomez, M. E., Yang, L., Levy Zamora, M., Hu, M., Lin, Y., Peng, J., Guo, S., Meng, J., Li, J., Cheng, C., Hu, T., Ren, Y., Wang, Y., Gao, J., Cao, J., An, Z., Zhou, W., Li, G., Wang, J., Tian, P., Marrero-Ortiz, W., Secrest, J., Du, Z., Zheng, J., Shang, D., Zeng, L., Shao, M., Wang, W., Huang, Y., Wang, Y., Zhu, Y., Li, Y., Hu, J., Pan, B., Cai, L., Cheng, Y., Ji, Y., Zhang, F., Rosenfeld, D., Liss, P. S., Duce, R. A., Kolb, C. E., and Molina, M. J.: Persistent sulfate formation from London Fog to Chinese haze, Proc. Natl. Acad. Sci. USA, 113, 13630-13635, doi: 10.1073/pnas.1616540113, 2016.

Wang, J., Li, J., Ye, J., Zhao, J., Wu, Y., Hu, J., Liu, D., Nie, D., Shen, F., Huang, X., Huang, D. D., Ji, D., Sun, X., Xu, W., Guo, J., Song, S., Qin, Y., Liu, P., Turner, J. R., Lee, H. C., Hwang, S., Liao, H., Martin, S. T., Zhang, Q., Chen, M., Sun, Y., Ge, X., and Jacob, D. J.: Fast sulfate formation from oxidation of SO_2 by NO_2 and HONO observed in Beijing haze, Nat. Commun., 11, 2844, doi: 10.1038/s41467-020-16683-x, 2020.

Xue, C., Zhang, C., Ye, C., Liu, P., Catoire, V., Krysztofiak, G., Chen, H., Ren, Y., Zhao, X., Wang, J., Zhang, F., Zhang, C., Zhang, J., An, J., Wang, T., Chen, J., Kleffmann, J., Mellouki, A., and Mu, Y.: HONO Budget and Its Role in Nitrate Formation in the Rural North China Plain, Environ. Sci. Technol., 54, 11048-11057, doi: 10.1021/acs.est.0c01832, 2020.